Promising anode materials for alkali metal ion batteries: A case study on cobalt anti-MXenes

Subhadeep Banerjee,[1,2] Ankita Narwal,[1,3] Sandeep K Reddy,[4] and Sharma S. R. K. C. Yamijala[1,2,3,5,*]

1. Department of Chemistry, Indian Institute of Technology Madras, Chennai, 600036 India.
2. Centre for Atomistic Modelling and Materials Design, Indian Institute of Technology Madras, Chennai 600036, India.
3. Centre for Molecular Materials and Functions, Indian Institute of Technology Madras, Chennai 600036, India.
4. Centre for Computational and Data Science, Indian Institute of Technology Kharagpur, Kharagpur, West Bengal, 721302 India.
5. Centre for Quantum Information, Communication, and Computing, Indian Institute of Technology Madras, Chennai 600036, India.
* yamijala@iitm.ac.in

Abstract

There is a continuous demand for energy storage devices with high energy density in consumer electronics, electric vehicles, and the grid energy market. Although commercial lithium-ion batteries (LIBs) satisfy the current needs, the limited availability of raw materials and moderate specific charge capacities (SCC) of LIBS, motivated scientists to search for alternate anode materials for LIBs and also to find technologies beyond LIBs. In this work, we studied the potential of six Cobalt anti-MXenes (CoAs, CoB, CoP, CoS, CoSe, and CoSi), a class of newly discovered 2D materials, as anode materials for lithium, sodium, and potassium ion batteries (LIBs, NIBs, and KIBs). We found that these materials are good electrical conductors and have high adsorption stability for the alkali metal ions, which helps to prevent the formation of dendrites and increase the cycle life of the battery. They also show moderate to low migration energy barriers (MEBs), indicating the potential for faster charge-discharge kinetics. We also explained the slightly counter-intuitive result of observing low MEBs along with high adsorption stability. Furthermore, Co-anti-MXenes can adsorb multiple alkali atoms per formula unit, resulting in high specific charge capacities and low average anodic voltages. For example, as anode materials for lithium-ion batteries, CoP and CoSi have SCC values of 1075.4 mAh g^{-1} and 934 mAh g^{-1}, and anodic voltages as low as 0.28 V and 0.43 V, respectively. Moreover, even the maximally metallated Co-anti-MXenes did not show agglomeration tendency at room temperature. Also, the volume expansion of these materials is minimum for both Li and Na adsorption. As a whole, we find that Co-anti-MXenes can act as promising anode materials for alkali metal ion batteries.

Introduction

Among the various kinds of energy storage systems, rechargeable batteries (specifically, lithium-ion batteries (LIBs)) gained significant interest due to their high storage capacity, less discharge time, and

long cycle life.[1–4] Due to their high energy density (100–265 Wh kg^{-1}), LIBs gradually captured the consumer and electronics market and, recently, the electric vehicle market.[5] However, the energy density of LIBs needs to be further improved to meet the requirements (> 350 Wh kg^{-1}) of long-range electric vehicles.[6] Also, to meet the ever-increasing global energy needs, the limited and unequal distribution of LIB raw materials (like lithium, nickel, and cobalt) demands sustainable alternatives.[7–11]

Among the alternatives to LIBs, sodium (Na) and potassium (K) ion batteries (NIBs and KIBs, respectively) have garnered significant attention for various reasons.[12] First of all, since lithium, sodium, and potassium belong to the same group in the periodic table, their electrochemical behavior is approximately similar. Secondly, since sodium and potassium have just 330 mV and 110 mV lower potential than Li ($E^0_{Na^+/\,Na}$ = -2.71 V, $E^0_{K^+/K}$ = -2.93 V, and $E^0_{Li^+/\,Li}$ = -3.04 V),[13] the anodic potentials of NIBs and KIBs are very close to that of LIBs. Thirdly, since the ionic radii of Na and K are larger than the Li (K^+ (1.33 Å) > Na^+ (0.97 Å) > Li^+ (0.68 Å)), they both have lower polarizing power ($\propto$ charge/radius) than Li ($Li^+ > Na^+ > K^+$). Consequently, in an electrolyte, Na^+ and K^+ ions can diffuse more quickly than the Li^+ ions,[14] providing faster charge-discharge rates in an electrochemical cell. Finally, both Na and K are earth-abundant (among the most abundant elements on the earth's crust, Na, K, and Li are in the 6th, 8th, and 33rd positions, respectively) and they are relatively evenly distributed on the globe.[15] Despite these promising characteristics of sodium and potassium, the current energy densities of NIBs and KIBs are still lower than their LIB counterparts.[16] To further improve the energy densities of these "*alkali metal ion batteries*" (alkali metal = Li, Na, and K), novel electrode and electrolyte materials need to be discovered.[17,18]

Earlier research showed that layered materials could be promising anode candidates for alkali metal ion batteries (AMIBs).[19–22] These layered materials are composed of stacks of novel 2D materials like graphene, borophene, phosphorene, transition metal dichalcogenides (TMDs), transition metal carbides, and carbonitrides (MXenes), or their hybrids.[23–26] Recently,[27] Gu et al. discovered a new class of materials called anti-MXenes, with promising electrochemical and catalytic applications. In these materials, the metal atomic layer is sandwiched between two nonmetal atomic layers (see **Figure 1a** and **Figure 1b**), an arrangement that is exactly opposite to the arrangement in MXenes, hence the name anti-MXenes. Gu et al. found 24 stable anti-MXenes, and they reported that CoB and FeB anti-MXenes could act as anode candidates for LIBs with high specific charge capacities (1099 and 1136 $mAhg^{-1}$, respectively).[27] Furthermore, in a recent study,[28] our group found that three cobalt anti-MXenes (Co-anti-MXenes), namely, CoB, CoP, and CoS are potential anode materials for NIBs.

Inspired by these findings, in this work, we studied six Co-anti-MXenes as anode candidates for AMIBs. To this end, using density functional theory, we computed various electrochemical properties such as specific charge capacity (SCC), anodic voltage, metal atom diffusion energy barrier, and others. We have also used some of our earlier results on NIBs[28] while comparing the performance of Co-anti-MXenes for different AMIBs. Our simulations show that Li and Na atoms bind moderately (adsorption energies are in the range of -0.79 to -1.7 eV) to the Co-anti-MXenes, whereas K atoms bind strongly (-1.26 to -2.22 eV). The migration energy barriers for alkali metal atoms are in the range of 0.2-0.8 eV, where the lowest barriers are observed for K atoms. The anodic voltages of Co-anti-MXenes are low for the Li and Na atoms (0.2-0.64 V) and slightly high for K atoms (0.6-1.2 V). Also, Co-anti-MXenes exhibited quite high SCC values for LIBs (1075 $mAhg^{-1}$, CoP) and NIBs (586 $mAhg^{-1}$,

CoS) respectively, but are slightly low (151─246 $mAhg^{-1}$) for KIBs. Interestingly, the observed SCC values for LIBs and NIBs are superior to many other 2D materials like graphite,[19] MoS_2,[29] and MXenes.[30] Together, from these results, we find that Co-anti-MXenes are promising anode candidates for LIBs and NIBs and reasonably good candidates for KIBs.

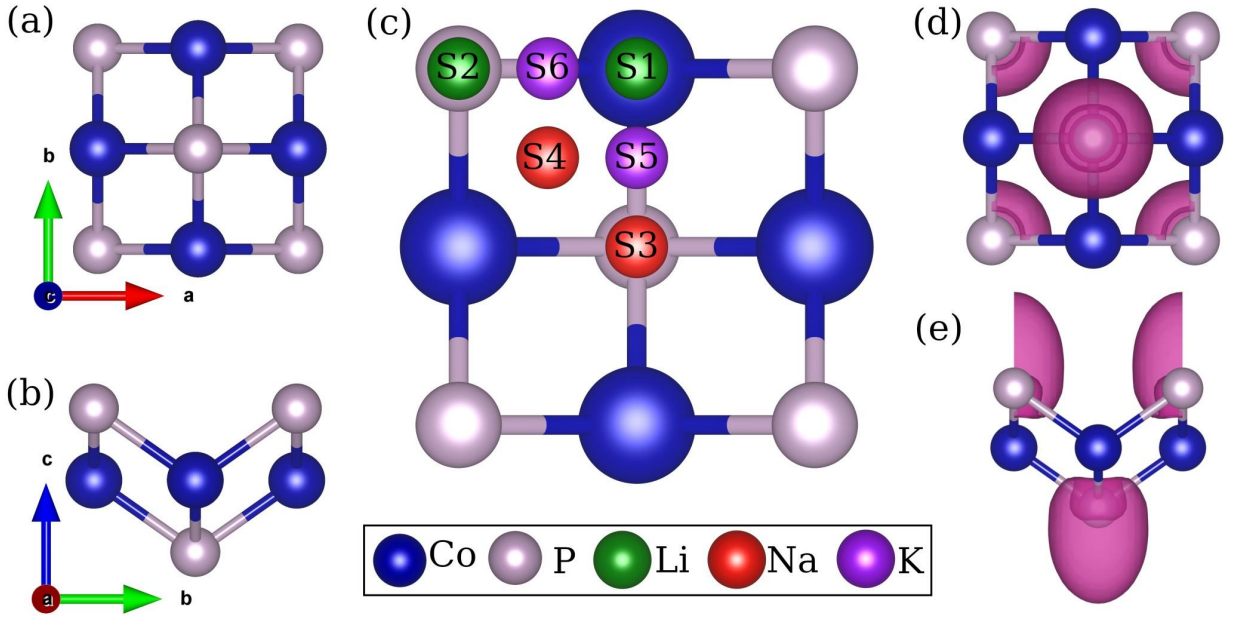

Figure 1. (a) Top and (b) side views of the optimized CoP structure. Each Co (P) atom is bonded to four P (Co) atoms. (c) various adsorption sites (depicted as S1-S6, see text for more details) for M (Li, Na, K) atoms on a CoP anti-MXene that we considered in this study, and (d) top and (e) side views of the electron localization function (ELF) plot of the CoP structure. The electrons are localized on the P atom, indicating an ionic-type interaction between Co and P. An isosurface value of 0.5 $e Å^{-3}$ is used for the ELF plot.

Computational Details

All first-principles calculations were performed based on the Kohn-Sham density functional theory using the projector augmented wave (PAW) method[31] as implemented in the Vienna ab initio simulation package (VASP).[32] The exchange and correlation interactions between the electrons were calculated within the generalized gradient approximation (GGA)[33] using the Perdew-Burke-Ernzerhof (PBE)[34] functional. For all the elements, we considered the standard valence configurations; Cobalt: $3d^8 4s^1$, Arsenic: $4s^2 4p^3$, Boron: $2s^2 2p^1$, Phosphorous: $3s^2 3p^3$, Sulfur: $3s^2 3p^4$, Selenium: $4s^2 4p^4$, Silicon: $3s^2 3p^2$, Lithium: $2s^1$, Sodium: $3s^1$, and Potassium: $3p^6 4s^1$. A 450 eV kinetic energy cutoff was used for the plane-wave basis set, and the dispersion interactions were included using the DFT-D3 method along with the Becke-Johnson damping function.[35] In all the calculations, to avoid any spurious interaction between the periodic images, the cell length along the z-direction was considered to be 40 Å.

To perform the structural relaxation, *ab initio* molecular dynamics, and multilayer adsorption studies, we considered a unit cell and sampled the Brillouin zone using a gamma-centered 12×12×1 k-mesh. For the density of states (DOS) calculations, a 25×25×1 k-mesh was used. The convergence criteria for energies and forces were kept as 10^{-5} eV and 0.02 eV/Å, respectively. For calculating the metal atom adsorption energies, charge density differences, charge analysis (Bader, Löwdin, and Mulliken), and metal atom diffusion energy barriers, a 3×3×1 supercell was considered along with a 4×4×1 k-mesh. The diffusion energy barriers were evaluated using the climbing-image nudged elastic band (CI-NEB)[36] method implemented in the VASP code.[37] The dynamical stability of the Co-anti-MXenes was studied using the phonon dispersion calculations within the finite displacement method[38] as implemented in the phonopy package.[39] The thermal stability was investigated by running a 15 ps long *ab initio* molecular dynamics (AIMD) simulation in an NVT (canonical) ensemble with a 1 fs timestep. The temperature of the NVT ensemble was maintained at 300 K using the Nosé–Hoover thermostat.[40] Finally, since oxides and sulfides of certain 3d metal atoms are known to possess strong correlations between electrons, accurately predicting their properties using DFT can be challenging. For this reason, we recalculated some of the properties of Co-anti-MXenes using the DFT+U method, where we varied the Hubbard parameter U from 1 eV to 6 eV. In these calculations, we used the geometries obtained at the PBE level of theory.

We used VASPKIT and pymatgen programs to obtain the relevant post-processing data, and the density of states and bandstructure were plotted using in-house python scripts.[41,42] All the optimized structures, electron localization functions, and charge-density difference maps were visualized using VESTA.[43]

Results and Discussion

Structural stability and electronic properties of pristine cobalt anti-MXenes

Since Jixing et al.[27] already discussed the structural properties of various anti-MXenes in detail, here, we briefly discuss the structural properties of Co-anti-MXenes. The top and side views of the optimized cobalt phosphide (CoP) anti-MXene are shown in **Figures 1a** and **Figure 1b**, respectively. The optimized geometries of other Co-anti-MXenes also look similar.[28] As shown in these figures, in an anti-MXene, each Co (X) atom is tetra coordinated with other X (Co) atoms, and the metal atoms are sandwiched between two atomic layers of nonmetals. As reported in our earlier work,[28] the calculated bond distances and layer thicknesses are in excellent agreement (within 0.36% and 1.14%, respectively) with the earlier report.[27] Similarly, in agreement with Gu's work,[27] the phonon band structures of all Co-anti-MXenes show only positive frequencies (see **Figure S1**), proving their dynamical stability. To understand the bonding nature between the Co and X atoms, we plotted the electron localization functions (ELF). From the ELF plots in **Figures 1d** and **1e**, it can be seen that the electron pair density is accumulated near the nonmetal atoms, indicating an ionic interaction between Co and P atoms, which stabilizes these systems. Similar results were obtained for other Co-anti-MXenes.[28]

To understand the electronic properties of Co-anti-MXenes, we calculated their electronic band structure and spin-polarized projected density of states (PDOS). Although we presented these results in an earlier article,[28] we are reiterating them here due to their significance in the current study. As shown in **Figure S2**, the conduction and valence bands of all these systems cross at the Fermi level. Similarly, all the PDOS plots have a finite density of states at the Fermi level, indicating the metallic nature of the Co-anti-MXenes (i.e., they are good electrical conductors). Further analysis (see **Figure S3**) suggests that the metallicity of Co-anti-MXenes stems from the Co d-orbitals. Considering the metallic character of Co-anti-MXenes, we further studied their feasibility as anode candidates for AMIBs. First, we discuss the Li/Na/K-atom's adsorption properties on these surfaces.

Adsorption energies of alkali metal atoms

It is important to note that during the charging process of a battery, metal atoms adsorb onto the anode surface, and during the discharging process, they desorb. As such, a good anode material should be able to adsorb metal atoms strongly, but at the same time, it should provide a lower diffusion barrier for the metal atoms.

In this work, we calculated the adsorption energy of a Li/Na/K-atom on a pristine 3✕3–CoX surface as $E_{ads} = E_{M+CoX} - E_{CoX} - E_M$, where E_{M+CoX} is the energy of the CoX surface along with the adsorbed alkali metal atom, E_{CoX} is the energy of the pristine CoX surface, and E_M is the energy of a single alkali metal atom (M= Li, Na, and K) in its bulk bcc lattice. As shown in **Figure 1c**, for metal atom adsorption on a Co-anti-MXene, there are six possible sites. We named them from S1 to S6, where the S1 site corresponds to the adsorption on top of the Co atom, S2: on top of the top-layer X atom, S3: on top of the bottom-layer X atom, S4: on top of the hollow site of the Co_2X_2 square, and S5 (S6): on top of the bridge between Co and bottom (top) layer X atom bond. Among these six sites, alkali metal atom adsorption is found to be thermodynamically feasible (i.e., with negative adsorption energy) only at three sites, namely, S1, S2, and S3, for all Co-anti-MXenes.

Table 1. The adsorption energy of a single Li/Na/K atom at the S1, S2, and S3 sites of a 3✕3 supercell of Co-anti-MXenes.

System	E_{ads} (eV), Li			E_{ads} (eV), Na			E_{ads} (eV), K		
	S3	S1	S2	S3	S1	S2	S3	S1	S2
CoAs	***-1.330***	-0.694	-0.065	***-1.226***	-0.771	-0.373	***-1.701***	-1.357	-1.044
CoB	***-1.642***	-1.225	-0.855	***-1.704***	-1.389	-1.124	***-2.178***	-1.984	-1.821
CoP	***-1.699***	-1.226	-0.643	***-1.694***	-1.315	-0.929	***-2.219***	-1.905	-1.600
CoS	***-0.958***	-0.554	0.115	***-0.967***	-0.565	-0.106	***-1.534***	-1.186	-0.835
CoSe	***-0.916***	-0.270	0.364	***-0.786***	-0.361	-0.003	***-1.265***	-0.888	-0.559
CoSi	***-1.527***	-0.710	0.031	***-1.371***	-0.779	-0.273	***-1.685***	-1.274	-0.926

As shown in **Table 1**, the Li/Na/K-atom's adsorption stability across all Co-anti-MXenes follows the order: S3 > S1 > S2. In agreement with this stability order, we find that the height of the Li/Na/K-atom from the Co-anti-MXene surface follows the order: S3 < S1 < S2 (see **Table S1**), i.e., the stronger the adsorption of a metal atom, the lower is its height from the Co-anti-MXene surface. Further, from the Bader charge analysis (see **Table S2**), we find that the Li/Na/K-atom donates about one electron to the Co-anti-MXene surface, suggesting that the alkali metal atoms are in a ~+1 charged state on these surfaces. However, since the differences in the charges on Li/Na/K-atom across the S1, S2, and S3 sites are less than 0.05 e^-, we could not find any clear correlation between the adsorption strength and the Bader charges. For comparison, we also computed the Mulliken and Löwdin charges for the Li/Na/K-atom adsorption at the S3 site. Our results (see **Table S3**) suggest that the charges predicted using all three schemes are approximately the same. While the differences between the Bader and Löwdin charges are quite insignificant (between 0–0.1 e^-), the Mulliken charges on the alkali metal atoms are slightly larger (by 0.3 e^-) than the Bader or Löwdin charges. For example, Bader and Löwdin schemes predict a charge of +0.8–1 for alkali metal atoms, whereas Mulliken's scheme predicts the charge to be between +0.9–1.2.

To further understand the adsorption stability order, we plotted the charge density differences (CDDs), where the CDDs are calculated as $\Delta\rho(MCoX) = \rho(MCoX) - \rho(CoX) - \rho(M)$, *where* $\rho(MCoX)$, $\rho(CoX)$, and $\rho(M)$ are the total electron densities of the 3×3-CoX surface along with the metal atom, pristine 3×3-CoX surface, and the single metal atom in the same supercell, respectively. The CDD plots (see **Figures 2** and **S4**) readily explain the higher adsorption energy of a Li/Na/K-atom at the S3 site over the S1 and S2 sites. As depicted in these plots, at the S3 site, the charge donated by the alkali metal atom is shared with four nonmetal atoms, creating a stronger interaction between the metal atom and the surface. On the other hand, at the S1 and S2 sites, this charge is shared with only two and one non-metal atoms, respectively, explaining the weaker adsorption energy at these sites. Hereafter, when we refer to the adsorption energy, we only refer to the adsorption at the S3 site (unless stated otherwise). Further, since the ionization potential decreases as we go down the periodic table, K-atom can share its electrons easily with the non-metal atoms when compared to the Na or Li atoms. Accordingly, the adsorption energies of the Li, Na, and K-atoms on any Co-anti-MXene surface follow the order: K > Na > Li.

As given in **Table 1**, the adsorption energies of Li/Na/K-atoms on all Co-anti-MXenes are negative at the S3 site, indicating that the adsorption process ($M + CoX \rightarrow MCoX$) is exothermic. Further, the Li, Na, and K adsorption energies lie within the ranges of -0.92 to -1.7 eV, -0.79 to -1.7 eV, and -1.26 to -2.22 eV, respectively, suggesting their chemisorption.[44] Interestingly, several 2D materials that are being used as anodes in experiments also have alkali metal atom adsorption energies in these ranges. For example, the adsorption energy of a Li-atom on Ti_2CO_2[45,46] and Ti_3C_2[47,48] MXenes is -1.55 eV and -0.504 eV energies, respectively, and on B_2N, B_3N, and B_5N surfaces, it is -1.67 eV, -0.81 eV, and -1 eV, respectively.[49,50] Similarly, the Na-atom adsorption energies on $Ti_3C_2O_2$ (-0.83 eV),[51,52] $Hf_3C_2F_2$ (-0.91 eV)[53,54] MXenes, and on rutile TiO_2 (-0.61 eV),[55,56] and MoS_2 (-0.77 eV)[57,58] are well within the adsorption energy range that we reported here for Co-anti-MXenes. The same is true also with the K-atom adsorption energies: Ti_3CNT_2 (T = OH: -2.1 eV, T = O: -2.27 eV, T = F: -2.04 eV)[59,60], Ti_3C_2 (-1.9 eV)[61,62], MoS_2 (~ -1.6 eV).[63,64] Together, the adsorption energy results indicate that Co-anti-MXenes could be promising anode materials for AMIBs.

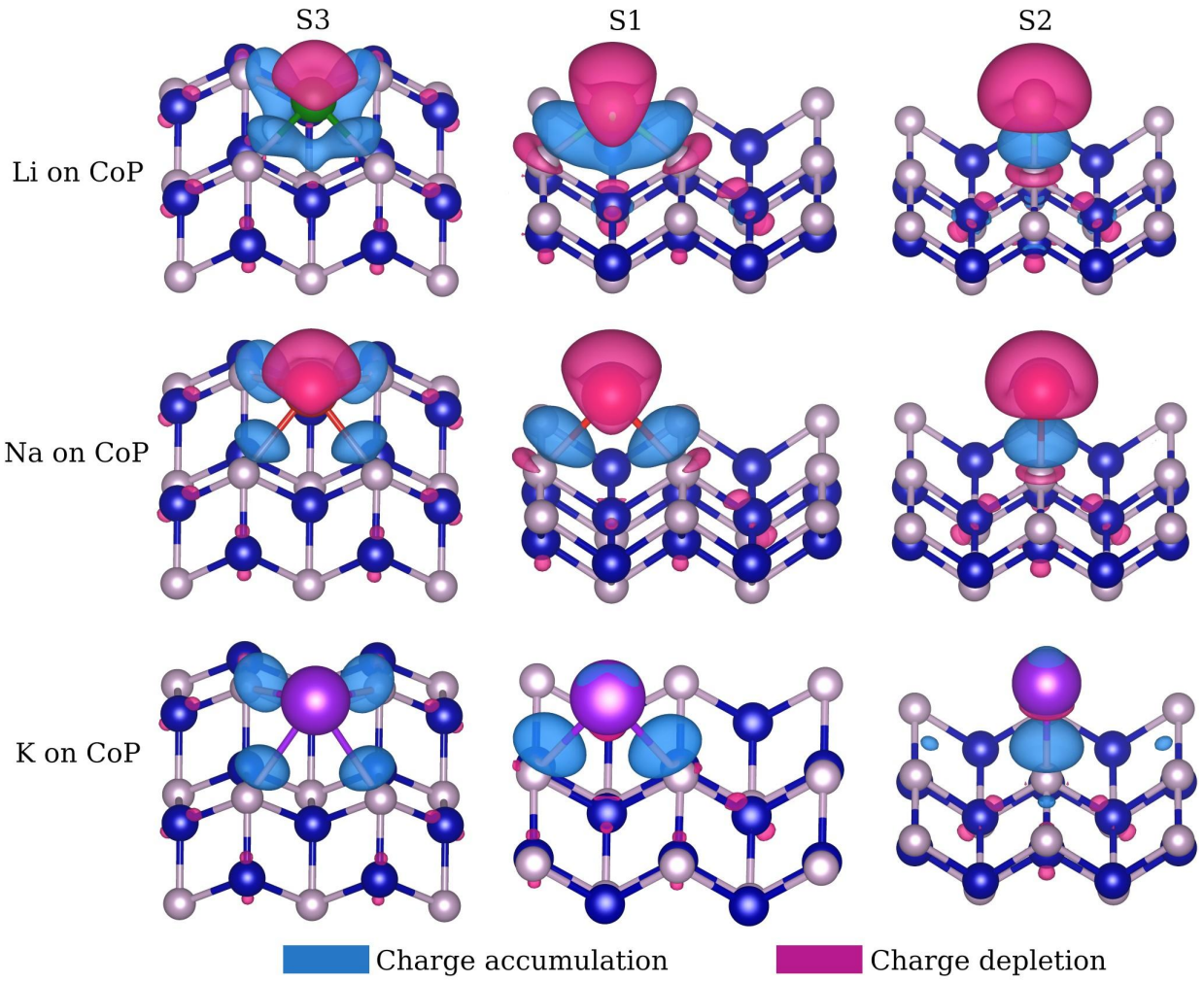

Figure 2. Charge density differences (CDDs) of a Li/Na/K-atom adsorbed at the S3, S1, and S2 sites of a CoP anti-MXene surface. Atom colors are the same as in Figure 1. Similar CDD plots on other Co-anti-MXene surfaces are shown in **Figure S4**. The magenta (sky-blue) color depicts the charge depletion (accumulation). The adsorbed metal atom interacts with four, two, and one nonmetal atoms at the S3, S1, and S2 sites, respectively, explaining the adsorption stability order (S3> S1> S2). An isosurface value of 0.002 e/$Å^3$ is used in all plots.

Migration energy barriers

It is desirable to have an electrochemical cell that can be charged quickly, and for quick charging, often the rate-limiting step is the ionic diffusion on the electrode surface. This is because the electrical conductivity (through the outer circuit) is larger than the ionic conductivity (through the solution), and ionic conductivity is larger in the electrolyte than on the electrode surface.[13,65] As such, for a faster charging process, a lower diffusion barrier for ion migration on the electrode surface is essential.

Here, we calculated the diffusion or migration energy barriers (MEBs) for Li, Na, and K atoms on the 3×3 supercells of Co-anti-MXenes using the CI-NEB method. As mentioned in the earlier section,

the S3 site is the most favorable site for the Li/Na/K-atom's adsorption, and accordingly, it is expected that the majority of the metal atoms would be adsorbed at these S3 sites. Further, the diffusion process can be visualized as the movement of a metal atom from one stable S3 site to another S3 site. As shown in **Figure 3a**, for this diffusion process, there are three possible paths, namely path-1, path-2, and path-3. Among these three paths, the CI-NEB results converged only along path-1 and path-3 (path-2 always converged to path-1), and as shown in **Figure 3b,** the diffusion barrier along path-1 is lower than along path-3. Although the results shown in **Figure 3b** are for the K-atom diffusion on the CoS surface, we obtained similar results (not shown) for the diffusion of Li and Na atoms as well.

The differences in the diffusion barriers along paths 1 and 3 can be understood by referring to the CDD plots (see **Figure 2** and **Figure S4**). Along path-1, the metal atom shares its electrons first with four S atoms (at the initial S3 site), next with two S atoms (at the S1 site), and finally again with four S atoms (at the final S3 site). On the other hand, along path-3, first, it shares with four S atoms (initial S3 site), next with only one S atom (S2 site), and finally again with four S atoms (final S3 site). Since the metal atom binds more strongly at the S1 site than at the S2 site, path-1 has less barrier for metal atom diffusion. In other words, the metal atom experiences only minimal changes in its adsorption/binding energy to the CoX surface while moving along path-1, as the difference in the adsorption energies between the S3 and S1 sites is smaller than that between the S3 and S2 sites. Consequently, the barrier for its migration along path-1 is low. Further elaboration on this concept is provided later in this section.

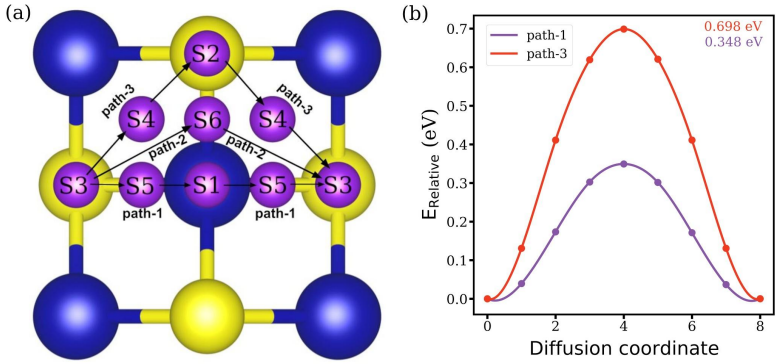

Figure 3. (a) Three possible diffusion paths for the alkali metal atom diffusion on the CoS surface. (b) K-atom diffusion energy barrier on the CoS surface along paths 1 and 3.

After establishing that path-1 is the most feasible path for the alkali-metal atom diffusion, we calculated the MEB values for the Li-, Na-, and K-atoms across all Co-anti-MXenes along this path, and the results are shown in **Figures 4a, 4b, and 4c**, respectively. From these results, it is clear that on any CoX surface, the MEB values follow the order: Li > Na > K, i.e., the potassium atoms diffuse more quickly than the sodium or lithium atoms. At first glance, this result might look counter-intuitive since a K-atom has stronger adsorption energy than the Li- or Na-atoms at all the sites along path-1 on any CoX surface (for a comparison of the adsorption energies of Li, Na, and K-atoms at the S3 and S1 sites, see **Table 1**). Here, the rationale would be "since a K atom is adsorbing strongly, it requires a large amount of energy (than a Li/Na atom) to remove it from the CoX surface, and accordingly, its MEB value should be high". However, this argument is not valid since, while moving a metal atom on the surface, we are not

completely removing it from that surface. Rather, we are just moving it from one site of the surface to another site (for example, from S3 to S1). Therefore, to estimate the MEB, instead of considering the *absolute potential* felt by the metal atom at the adsorption sites, we just need to consider the *difference in the potential* felt by the metal atom at these sites (equivalent to the adsorption energy differences at these sites). Accordingly, *if the difference in the adsorption energies of a metal atom at two sites is large (small), then the MEB for its diffusion between these two sites would be high (low)*. Obviously, we must consider the adsorption energies of the metal atom at the intermediate sites (if any) between the two sites of our interest. Finally, if the adsorption energies of a metal atom at all sites of a surface are the same, then there should be no barrier to its diffusion (since the atom is moving on a constant potential).

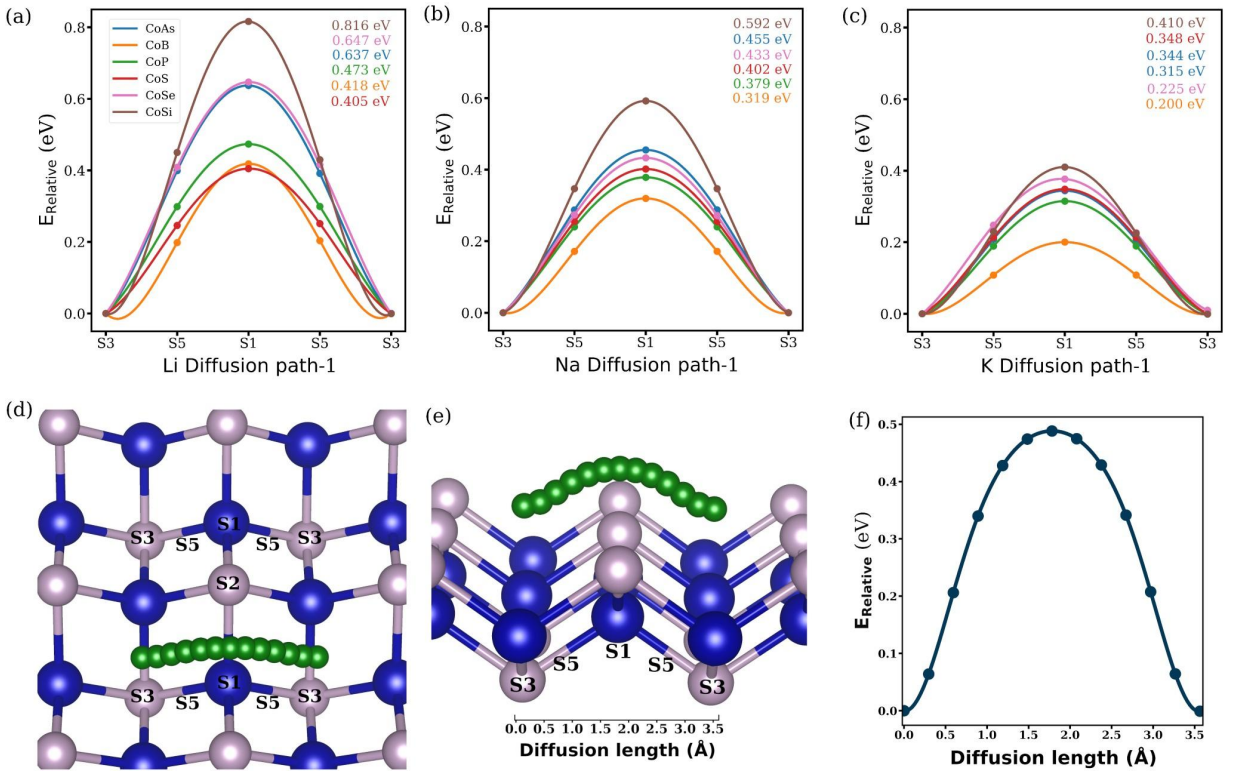

Figure 4. MEB values for the (a) Li-, (b) Na-, and (c) K-atoms across all Co-anti-MXenes along the path-1. The MEB values follow the order: Li > Na > K, i.e., a potassium atom diffuses quickly on all the Co-anti-MXene surfaces when compared to a Li or Na atom. (d) and (e) shows the top and side view of Li diffusion through path-1 on the CoP surface, (f) is the relative Li atom adsorption energies at various adsorption sites through its diffusion path. **Figure 4b** is adapted from reference 28 with permission.[28] (Copyright © 2022, American Chemical Society).

A pictorial representation of our hypothesis is given in **Figures 4d, 4e, and 4f**, where we presented the changes in the adsorption energy of a Li-atom while it is moving from one S3 site to another S3 site (path-1) on the CoP surface. In these calculations, to ensure that the Li-atom moves only along path-1, we only allowed the optimization of Li-atom's z-coordinate. By comparing **Figures 4a and 4f**, it is apparent that the Li-atom's MEB on the CoP surface (along path-1) is roughly equal to the difference in the Li-atom's adsorption energy between the S3 and S1 sites, which validates our hypothesis. Our hypothesis can be readily used to explain the differences in the MEBs of (i) a metal atom along different

paths (i.e., why path-1 has lower MEB than path-3) on a CoX surface, (ii) different alkali metal atoms on a specific CoX surface (i.e., why a K-atom has lower MEB than a Li/Na-atom on the CoS surface), and (iii) the same metal atom across different CoX surfaces. For example, as given in **Table 1**, the difference in the adsorption energies between the S3 and S1 sites on all CoX surfaces follow the order: Li > Na > K. Therefore, according to the above analysis, the K-atom should possess the least MEB value, and it does. Similarly, the adsorption energy differences between the S3 and S1 sites for a Li-atom on the CoX surfaces follow the order: CoSi > CoSe > CoAs > CoP > CoB > CoS, which exactly matches the order of the MEB values for the Li-atom on these surfaces calculated using CI-NEB. It is important to note that although K has the least MEB value, its larger inertia (due to its larger mass) may also make it less likely to move as quickly as the lighter atoms. However, once K is set in motion (for example, due to external forces such as an applied voltage or an increase in temperature), it will experience the least resistance to its movement, compared to Li or Na.

Finally, by comparing the MEB values of Li/Na/K on Co-anti-MXenes with the existing anode materials, we find that Co-anti-MXenes can act as superior anode materials for AMIBs. For example, the MEB values of Li (0.41–0.82 eV) on Co-anti-MXenes are lower than the commercial Li-graphite batteries (0.45-1.20 eV),[66] and are comparable to other 2D materials like $Hf_3C_2O_2$ (0.62 eV) and $Zr_3C_2O_2$ (0.53 eV) MXenes,[67] MoN_2 (0.78 eV),[68] β_{12} (0.6 eV) and χ_3 (0.66 eV) borophenes,[69] and phosphorene (0.76 eV).[70] Similarly, the MEB values of Na (0.32–0.59 eV) on Co-anti-MXenes are either superior or comparable to the other 2D materials like $Hf_3C_2O_2$ (0.36 eV) and $Zr_3C_2O_2$ (0.28 eV) MXenes,[67] MoN_2 (0.56 eV),[68] β_{12} (0.33 eV) and χ_3 (0.34 eV) borophenes,[69] and T-graphene (0.35 eV).[71] The reported MEB values for K atom on various 2D materials are: $Hf_3C_2O_2$ (0.21 eV), $Zr_3C_2O_2$ (0.17 eV),[67] MoN_2 (0.49 eV),[68] and T-graphene (0.25 eV).[71] Apparently, these values are comparable to the MEB values that we obtained for K (0.2–0.41 eV) on Co-anti-MXenes. Together, we conclude that *due to their low MEBs for Li, Na, and K-atoms, Co-anti-MXenes can serve as fast-charging anode materials for AMIBs*.

Multilayer alkali metal atom adsorption

Until now, we studied the properties of a single metal atom adsorption and diffusion. However, in a real battery, multiple metal atoms would be adsorbed onto the anode. In this section, we calculated the maximum number of Li/Na/K-atoms that can be adsorbed on each of the Co-anti-MXene. These maximally metallated configurations would be used in the later sections to calculate the average metalation voltage and the specific charge capacity (SCC).

Table 2. Layer-wise average adsorption energy (eV) values of alkali metal atoms on various CoX surfaces. For each CoX surface, the average adsorption energy for the configuration with the maximum number of metal atoms (see text for more details) is shown in bold.

Systems	**Li**						**Na**					**K**	
	$\Delta E_{ads.}^{L1}$ (eV)	$\Delta E_{ads.}^{L2}$ (eV)	$\Delta E_{ads.}^{L3}$ (eV)	$\Delta E_{ads.}^{L4}$ (eV)	$\Delta E_{ads.}^{L5}$ (eV)	$\Delta E_{ads.}^{L6}$ (eV)	$\Delta E_{ads.}^{L1}$ (eV)	$\Delta E_{ads.}^{L2}$ (eV)	$\Delta E_{ads.}^{L3}$ (eV)	$\Delta E_{ads.}^{L4}$ (eV)	$\Delta E_{ads.}^{L5}$ (eV)	$\Delta E_{ads.}^{L1}$ (eV)	$\Delta E_{ads.}^{L2}$ (eV)
CoAs	**-1.093**	0.091	-	-	-	-	-0.730	-0.126	**-0.005**	-0.021	-	**-0.763**	0.137

CoB	**-1.431**	0.063	-	-	-	-	-1.107	-0.074	**-0.006**	-0.014	-	**-0.970**	0.207
CoP	-1.236	-0.086	-0.049	-0.036	**-0.015**	-0.021	-0.906	-0.116	**-0.001**	-0.023	-	**-0.928**	0.195
CoS	**-0.937**	0.067	-	-	-	-	-0.679	-0.077	-0.022	**-0.018**	-0.017	**-0.787**	0.171
CoSe	**-0.984**	0.268	-	-	-	-	-0.590	-0.060	**-0.015**	-0.017	-	**-0.610**	0.124
CoSi	-1.564	-0.110	**-0.04**	-0.027	-	-	-1.265	**-0.016**	-0.115	**-**	-	**-1.195**	0.141

Assuming a layer-by-layer adsorption of alkali metal atoms at the anode surface, the following reversible electrochemical reaction would occur during the charging process

$$M_mCo_2X_2 + (n - m)M^+ + (n - m)e^- \leftrightharpoons M_nCo_2X_2 \quad (1)$$

where 'M' represents the alkali metal atom (Li/Na/K) that is being adsorbed, 'm' represents the total number of alkali metals that were already adsorbed (say, up to the $(L-1)^{th}$ layer), and (n-m) is the number of newly adsorbed atoms (say, at the L^{th} layer). For the electrochemical reaction in **equation 1**, we calculated the average adsorption energy of an alkali metal atom at the L^{th} layer as

$$\Delta E^L_{ads.} = [E(M_nCo_2X_2) - E(M_mCo_2X_2) - (n - m)*E(M)] \,/\, (n - m) \quad (2)$$

where $E(M_nCo_2X_2)$ and $E(M_mCo_2X_2)$ are the energies of the Co_2X_2 unit cell with 'L' and 'L-1' layers of alkali metal atoms (M=Li/Na/K) adsorbed onto them, respectively, and $E(M)$ is the energy of a single metal atom in its bcc bulk structure. Here, it is important to note that we allowed the adsorption of metal atoms on both sides of the CoX surface. Accordingly, when we are referring to L-layers of adsorption, we are actually adsorbing 2L-layers of metal atoms ('L' layers above and 'L' layers below) onto the CoX surface. Also, it should be noted that the most stable site of adsorption changes from layer to layer. As noted earlier, at the first layer, S3 is the most stable site for metal atom adsorption. At the second layer, we find that S2 is the most stable site for all CoX systems except for the CoSi (on which S1 is the most stable site for Li atom adsorption). For the higher layers, this pattern repeats, i.e., for the third, fourth, fifth, and sixth layers, the stable adsorption sites are S3, S2, S3, and S2, respectively. The optimized structures of the maximally metallated Co-anti-MXenes with Li-, Na-, and K-atoms are shown in **Figure S5**, **Figure S6**, and **Figure S7**, respectively, and the layer-wise average adsorption energy values (calculated using **equation 2**) are given in **Table 2**.

In general, as the metal atom concentration increases on the CoX surface, due to the electrostatic repulsion between the metal atoms, the adsorption energy values slowly become less negative, and after a point, the adsorption process becomes thermodynamically prohibited. Accordingly, in our calculations, if we obtained a positive or near-zero adsorption energy value after adsorbing the L^{th} layer of metal atoms, then we considered that a maximum of "L-1" layers of metal atoms can be adsorbed onto a CoX surface. For example, as shown in **Table 2**, only one layer of Li atoms can be adsorbed onto the CoAs, CoB, CoS, and CoSe surfaces (on both sides). The same is true for the K atoms on all CoX surfaces. However, in some cases, the average adsorption energy (see equation 2) at the L^{th} layer can be more negative (i.e., stable) when compared to the $L\text{-}1^{th}$ layer. Such situations correspond to the agglomeration of metal atoms

(i.e., they lead to the formation of metal clusters) on the anode surface,[72] and in such cases, we again considered that a maximum of "L-1" layers of metal atoms can be adsorbed onto a CoX surface. Accordingly, as shown in **Table 2**, we can adsorb up to five layers of Li onto the CoP (again, both sides), three layers of Li onto the CoSi, two layers of Na onto the CoSi, and three layers of Na onto the CoAs, CoB, and CoP surfaces. In a few cases, the adsorption energy did not change much as we move from the L-1th layer to the Lth layer. Since such a result is physically less feasible, we only considered the adsorption till the "L-1" layers. This situation occurred while adsorbing Na atoms onto the CoSe and CoS surfaces, and we considered a maximum of three (four) layers of Na atom adsorption onto CoSe (CoS).

Metal-insertion voltage (V) and specific charge capacity (SCC)

Next, we studied two important electrochemical parameters, namely, metal-insertion voltage and specific charge capacity (SCC), that dictate the energy density of an electrochemical cell. The energy density (Wh/g) is defined as the product of SCC (mAh/g) and total cell voltage (V). Therefore, to obtain high energy densities, both SCC and total cell voltage values should be high. Moreover, since the total cell voltage is equal to the difference between the cathodic and anodic voltages, we need to keep the anodic (cathodic) voltage as low (high) as possible. *Therefore, an high energy density anode would possess a low anodic voltage (generally, 0.1-1 V is considered to be low)[73] and high SCC*.[28]

During charging, the anodic voltage is defined as the voltage at which the alkali-metal ions are inserted into the anode material. Hence, it is also known as the metal-insertion voltage and is calculated using the Nernst equation, $V = \frac{-\Delta G}{nF}$. Here, the Gibbs free energy change is estimated from the second law of thermodynamics as, $\Delta G = \Delta E^{L}_{ads.} + p\Delta V - T\Delta S$, where $\Delta E^{L}_{ads.}$ is defined as in **equation 2** and the corresponding values are given in **Table 2**. During the metal atom insertion process, the volume and entropy changes are quite small compared to the adsorption energy value, and they can be neglected.[74,75] Accordingly, we can approximate the metal-insertion voltage as $V = \frac{-\Delta E^{L}_{ads.}}{Z|e|}$, where 'Z' is the valence charge of the inserted metal atom (here, +1), and '|e|' is the fundamental charge (1.602×10^{-19} C). Also, since the ΔG should be negative for a spontaneous reaction, only negative $\Delta E^{L}_{ads.}$ values or positive metal-insertion voltage values are meaningful. A zero metal-insertion voltage indicates the maximum concentration of the metal atoms that can be adsorbed on a CoX surface, and a negative value suggests that metal atom adsorption at that concentration is thermodynamically not feasible. The calculated metal-insertion voltages (for various metal atom concentrations per CoX formula unit) for Li, Na, and K are shown in **Figures 5a, 5b, and 5c**, respectively. Apparently, in all cases, with an increase in the metal atom concentration, the metal-insertion voltage decreases and approaches zero.

As shown in **Figure 5a**, the average *lithiation voltages* of the Co-anti-MXenes are CoAs (1.09 V), CoB (1.43 V), CoP (0.28 V), CoS (0.94 V), CoSe (0.98 V), and CoSi (0.43 V). Only CoP and CoSi have metal-insertion voltages that are well below 1 V, and accordingly, they can be considered as suitable anode materials for LIBs. If CoP (CoSi) is used along with a traditional cathode material like $LiCoO_2$ or $LiMn_2O_4$ (with ~ 4 V cathodic voltage), it can give a total cell voltage of about 3.72 (3.43) V, which is close to the cell voltage of a commercial LIB (2.50–3.90 V).[76] The average lithiation voltages of CoP and

CoSi are superior to some 2D anode materials like B_xN (1.07 V, 0.54 V, 0.90 V, and 0.74 V for B_2N, B_3N, B_4N, and B_5N),[49] defective carbon nanocone (CNC, 0.59 V),[77] MXenes like $Hf_3C_2S_2$ (1.17 V),[72] Ti_3C_2 (0.62 V),[47] etc.

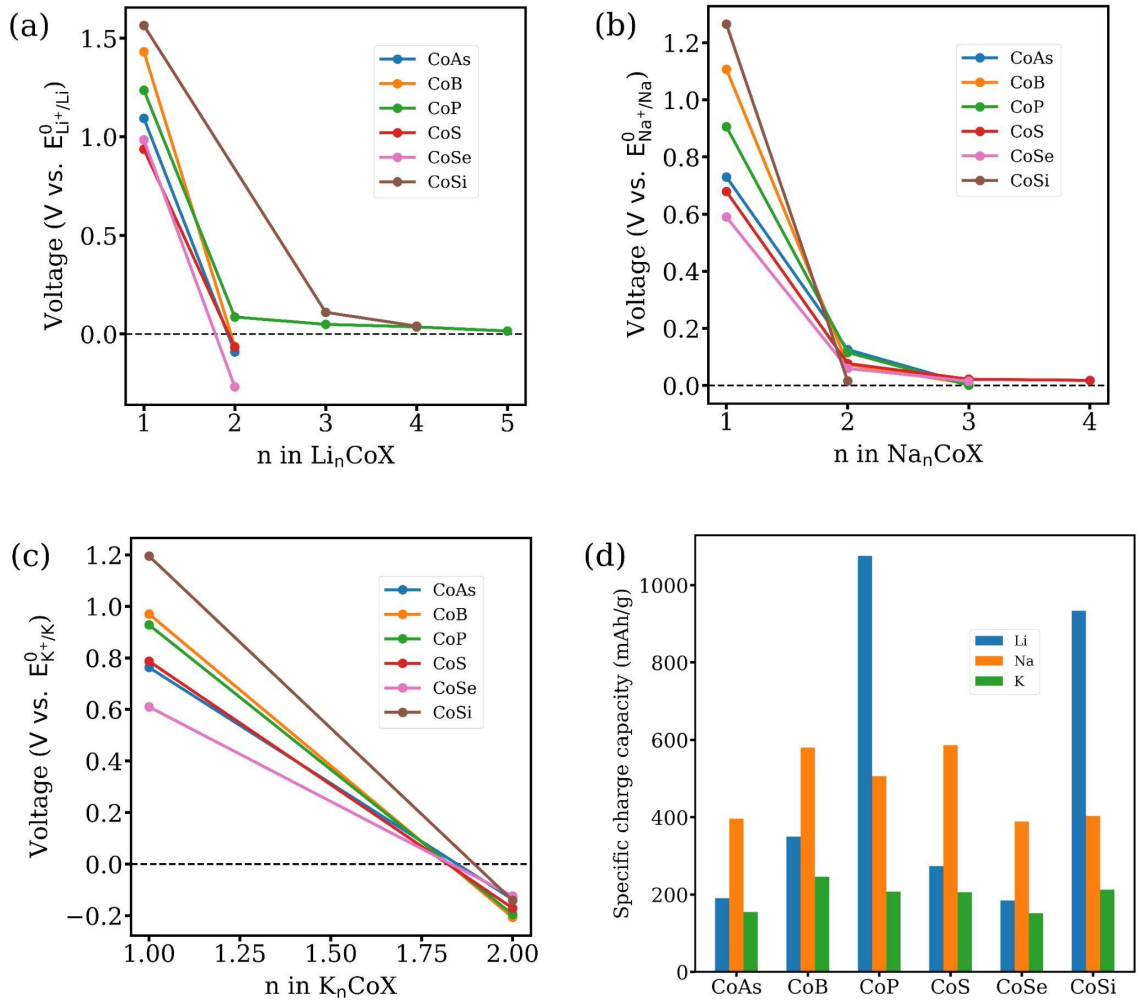

Figure 5. Calculated (a) Li, (b) Na, and (c) K-atom insertion voltages on various Co-anti-MXene surfaces with varying metal atom concentrations. With an increase in the metal atom concentration, the metal-insertion voltage decreases and approaches zero. A zero metal-insertion voltage indicates the maximum concentration of the metal atoms that can be adsorbed on a CoX surface, and a negative voltage suggests that metal atom adsorption at that concentration is thermodynamically not feasible. (d) SCC values for the maximally metallated structures. CoP, CoS, and CoB exhibited the highest SCC values for Li, Na, and K, respectively, and formed Li_5CoP, Na_4CoS, and KCoB. Figure 5(b) is reproduced from reference 28 with permission[28] (Copyright © 2022, American Chemical Society).

The average *sodiation voltages* of the Co-anti-MXenes (**Figure 5b**) are: CoAs (0.29 V), CoB (0.40 V), CoP (0.34 V), CoS (0.20 V), CoSe (0.22 V), and CoSi (0.64 V). These results were already reported in our earlier work, but are repeated here for comparison.[28] Apparently, unlike the lithiation voltages, the sodiation voltages of all Co-anti-MXenes are in the expected range (well below 1 V). When combined with a commercial cathode material like $Na_3V_2(PO_4)_3F_3$ or $NaNi_{0.68}Mn_{0.22}Co_{0.1}O_2$ (~ 4V), they can yield a total cell voltage of up to 3.80 V, on par with commercial LIBs and even superior to a few

SIBs.[78–80] Sodiation voltages of Co-anti-MXenes are comparable/superior to various materials like BC_3 (1.36 - 1.48 V),[81] Ti_2PX_2 for X = S, Se, and Te (0.4 - 0.6 V),[82] Ti_2B (0.29 V),[83] MXenes like $M_3C_2S_2$ (0.31 V for M = Ti, 0.46 V for M = Hf), Ti_3N_2 (0.51 V), $Ti_3N_2O_2$ (0.72 V),[84] etc. In **Figure 5c**, we depicted the average *potassiation voltages* of all Co-anti-MXenes. Only CoAs, CoS, and CoSe have reasonable voltages (0.76 V, 0.79 V, and 0.61 V, respectively). As such, unless we have high-voltage cathode materials (> 4 V), Co-anti-MXenes could only give the total cell voltages below 3.5 V for KIBs. However, it is worth noting that the anodic voltages that we obtained for Co-anti-MXenes are comparable/superior to several 2D materials like AsP (0.93 V),[85] defective phosphorene (~0.8 V),[86] B_3X (0.99 V for X = F, 1.05 V for X = Cl),[87] MoO_2 (0.75 V),[88] etc. As a whole, *based on the metal-insertion voltage values alone, we can suggest that all Co-anti-MXenes are promising anode materials for NIBs, CoP and CoSi are promising for LIBs, and CoAs, CoS, and CoSe are promising for KIBs.*

Next, we computed the SCC for maximally metallated structures (**Figures S5**, **S6**, and **S7**). SCC (mAh/g) is defined as the amount of charge that can be extracted from a gram of the anode material during the discharge process. Accordingly, it is calculated as, SCC = $\frac{nZF}{M.W.\,of\,M_nCoX}$, where 'n' is the number of alkali metal atoms adsorbed per formula unit of CoX, 'Z' is the valence charge of the inserted metal atom (here, +1), 'F' is the Faraday constant (26801.486 mAh/mol), and M.W. of M_nCoX is the molecular weight (g/mol) of the active material involved in the electrochemical reaction.[89] In general, since 'Z' and 'F' are the constant across the alkali metal atoms, the SCC value is directly proportional to 'n' and inversely proportional to the molecular weight of the 'M_nCoX'. Accordingly, for a fixed 'n', on a specific Co-anti-MXene, we should observe a maximum value of SCC for the lithium adsorption (due to its lightweight) followed by the sodium and potassium. Similarly, for a fixed 'n' and alkali-metal atom, the highest SCC will be obtained for the Co-anti-MXene with the lightest non-metal atom (here, CoB).

As shown in **Figure 5d**, for LIBs, the order of SCC values (along with the formula unit corresponding to the maximally metallated structures) is: Li_5CoP (1075 mAh/g) > Li_4CoSi (934 mAh/g) > LiCoB (349 mAh/g) > LiCoS (274 mAh/g) > LiCoAs (190 mAh/g) > LiCoSe (185 mAh/g). Clearly, since CoP (CoSi) can adsorb five (four) lithium atoms per formula unit, it has the highest SCC value. All others adsorbed only one lithium atom per formula unit, and among them, since CoB is the lightest compound it has the highest SCC. The SCC values of Co-anti-MXenes for LIBs are comparable/superior to many 2D materials: MXenes M_2C (93-337 mAh/g), and M_3C_2 (141-526 mAh/g) for M = Sc, Ti, V, Cr, Zr, Nb, Mo, Hf, Ta, and W,[90] MoS_2 (670 mAh/g),[29] graphite anode (372 mAh/g),[91] MBenes (968 mAh/g)[92], etc.

Similarly, as reported by us earlier,[28] for NIBs, the order of SCC values (along with the formula unit corresponding to the maximally metallated structures) is: Na_4CoS (586 mAh/g) > Na_3CoB (580 mAh/g) > Na_3CoP (506 mAh/g) > Na_2CoSi (403 mAh/g) > Na_3CoAs (396 mAh/g) > Na_3CoSe (389 mAh/g). The SCC values of CoS and CoB can be compared with other 2D materials like BC_3 (572 mAh/g),[81] hydrogenated defected graphene (591.2 mAh/g),[93] α-GeS (512 mAh/g)[94], MXene like $Ti_3C_2O_2$ (536 mAh/g),[67] etc. For KIBs, as shown in **Table 2**, all Co-anti-MXenes could only adsorb one K-atom per formula unit. Accordingly, the order of the SCC values is inversely proportional to the atomic weight of the nonmetals in the Co-anti-MXenes, i.e., KCoB (246 mAh/g) > KCoSi (213 mAh/g) > KCoP (208 mAh/g) > KCoS (206 mAh/g) > KCoAs (155 mAh/g) > KCoSe (151 mAh/g). The SCC value of CoB is comparable with some 2D materials like graphite (273 mAh g^{-1}),[95] Phosphorene (265.22 mAh/g),[96]

MXenes like V_3C_2 (269.86 mAh/g),[97], Ti_2CO_2 (264 mAh/g),[98], $Ti_3C_2S_2$ (231.43 mAh/g),[72] 2D TMDs $NiSe_2$ (247 mAh/g),[99] etc. As a whole, *based on the SCC values alone, we can suggest that CoP and CoSi are promising anode materials for LIBs, CoS, CoB, and CoP are promising for NIBs, and CoB, CoSi, CoP, and CoS are reasonably good for KIBs.*

Stability of the maximally metallated Co-anti-MXenes

Next, we studied the thermal and electronic stability of the maximally metallated Co-anti-MXenes. To check their thermal stability, we conducted a 15 ps NVT simulation at 300 K. Since these simulations are computationally expensive, we only studied the structures with high SCC values, namely, Li_4CoSi, Li_5CoP, Na_3CoB, Na_3CoP, and Na_4CoS. In **Figures 6b, and 6e**, we depicted the structures of Li_4CoSi and Li_5CoP after a 15 ps run. Clearly, both of these structures are thermally stable, i.e., neither we observed any agglomeration of the alkali metal atoms nor any structural distortion. Also, the energy fluctuations in these structures are negligible (~ 0.5 eV) throughout the NVT simulation. We observed similar results for the maximally sodiated structures (see **Figure S8**).[28]

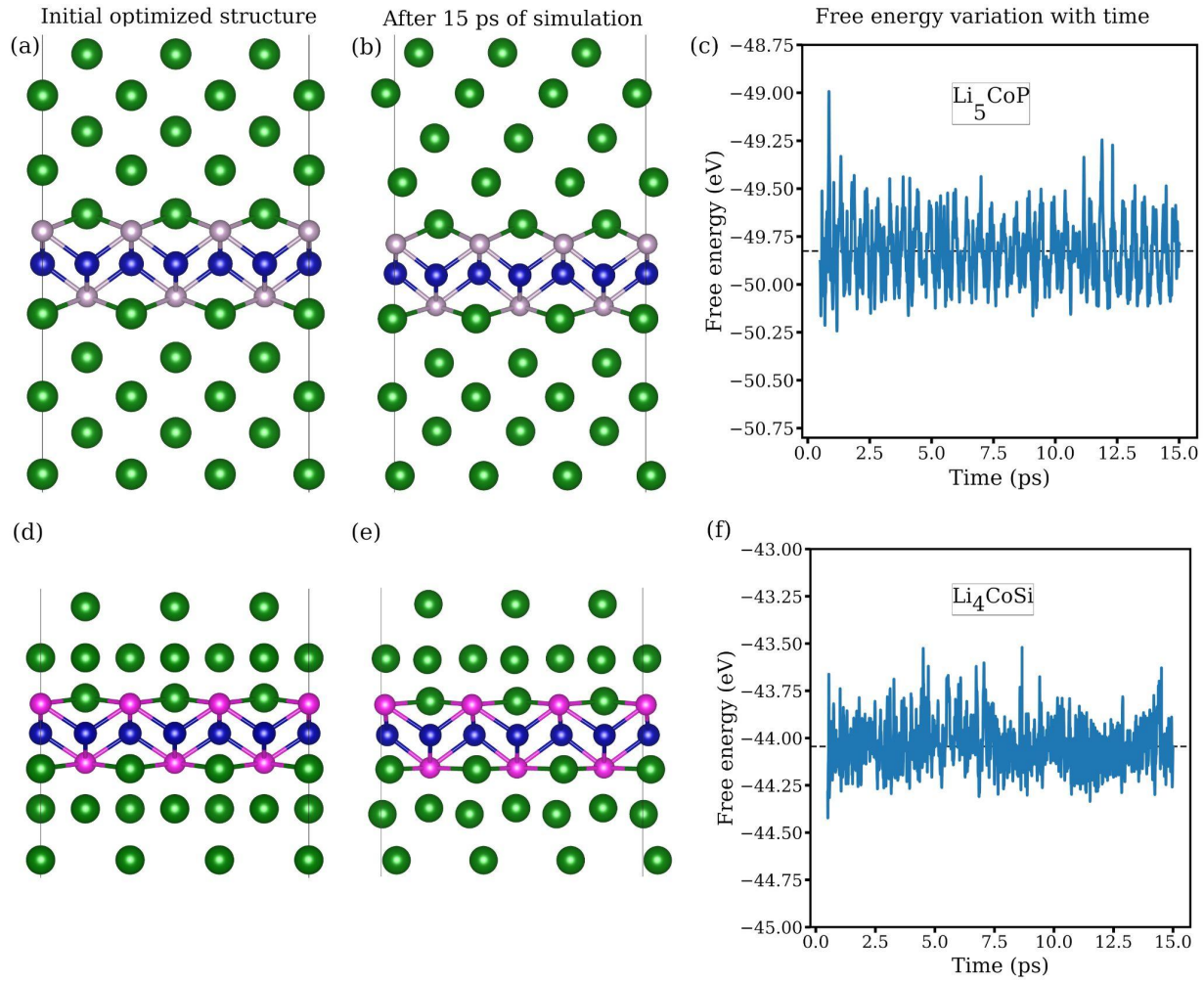

Figure 6. (a) and (d) depict the initial optimized structures of Li_5CoP and Li_4CoSi, respectively. (b) and (e) depict the corresponding structures after a 15 ps NVT simulation at 300 K. (c) and (f) show their free energy fluctuations during the simulation duration.

To check the electronic stability, we analyzed the electron localization functions (see Figures **S9** and **S10**) of all Co-anti-MXenes. For the single-layer adsorption, we observed a large electron density ($0.6 \leq ELF \leq 0.8$; yellow/red color) around the non-metal atoms, indicating a strong ionic interaction between the adsorbed alkali metal atoms and the nonmetal atoms of the Co-anti-MXene. For the multi-layer adsorption (observed only for lithiation and sodiation[28]), we observed a moderate electron density ($0.4 \leq ELF \leq 0.56$; green/yellow color) around the adsorbed alkali metal atoms, which decreases the metal-metal repulsive interactions and stabilizes the maximally metallated structures.[67,98] Additionally, to understand why multiple layers of potassium atoms cannot adsorb on Co-anti-MXenes, we analyzed the ELF plots of all Co-anti-MXenes with two layers of K atoms adsorbed onto them (see **Figure S11**). As shown in these plots, there is very little electron cloud (blue color) between the K atoms, which cannot screen the metal-metal repulsive interactions, indicating the reason for their instability. Together, *we conclude that the maximally metallated Co-anti-MXenes are quite stable*.

Finally, we also studied the expansion of the Co-anti-MXenes after the insertion of multiple layers of alkali metal atoms. For these studies, we considered the Co-anti-MXenes that gave the highest SCC values for each alkali metal ion. Accordingly, we studied the expansion of CoP (CoS) bilayers for Li (Na) intercalation. Since multi-layer adsorption of K atoms on Co-anti-MXenes is not thermodynamically feasible, we did not inspect their expansion. The optimized interlayer distances in pristine CoP and CoS are 2.219 Å and 3.155 Å, respectively. After a single Li (Na) atom intercalation, the CoP (CoS) bilayer expanded along the z-axis by 0.045% (0.86%), as shown in **Figure S12** (**Figure S13**). These expansions are negligible when compared to graphite, which expands by 15% (40%) for a single Li (Na) atom intercalation.[100] After intercalating five (four) layers of Li (Na^{28}) atoms into a CoP (CoS) bilayer, we observed an expansion of up to 276.03% (266.28%), which is comparable to the ~268% expansion observed in $Ti_3N_2O_2$ after intercalating five layers of Na atoms.[101] As such, the volume expansion of Co-anti-MXenes is comparable to a few 2D materials and is negligible compared to the commercial graphite anode material.

Effect of strong correlations

It is widely accepted that simulating materials with strongly correlated electrons is a challenging task for DFT, and several transition metal oxides and sulfides are known to exhibit these strong correlations. For this reason, we employed PBE+U simulations on Co-anti-MXenes to understand how our results (predicted at the PBE-level of theory) would be affected by the inclusion of "Hubbard U", which indicates the onsite repulsion between electrons occupying the same orbital. Since Co-anti-MXenes are not yet synthesized, there is no experimental bandstructure to verify our results against a particular U value. Consequently, we have varied the U value from 1 to 6 eV in 1 eV intervals and computed the adsorption energy, bandstructure, and magnetic moment for each of these U values. These results are presented in **Table 3, Figure S14,** and **Figure 7**.

We will first present the PBE+U results of the CoS system. As shown in **Figure S14**, although the bandstructure of CoS changed with the inclusion of U, the system remained metallic at all U values, indicating that it is a suitable electrode material. Moreover, the effect of U is only prominent on the β-spin states (the ∝-spin states were not affected much till U = 5 eV). By increasing the U value, there is a destabilization (stabilization) in the β-spin states (α-spin states, only at U= 6 eV); they slowly moved from the valence band region into the conduction band region. Similar to the metallicity, the magnetic moment also did not change significantly up to U=5 eV (see **Table 3**). However, at U=6 eV the magnetic moment increased by about four times. *Overall, we can conclude that the metallicity and magnetic moment of the Co-anti-MXenes will not be affected strongly for U values below 5 eV.*

Table 3. Changes in the adsorption energy (eV), and magnetic moment (Bohr Magneton) of the CoS unit cell with a variation in the Hubbard U value.

Property		**U = 0 eV (PBE)**	**U = 1.0 eV**	**U = 2.0 eV**	**U = 3.0 eV**	**U = 4.0 eV**	**U = 5.0 eV**	**U = 6.0 eV**
Adsorption energy (eV) at the S3 site	**Li**	-0.958	-1.011	-1.079	-1.586	-3.775	-5.270	-4.689
	Na	-0.967	-1.016	-1.075	-1.123	-3.975	-3.498	-4.208
	K	-1.534	-1.582	-1.634	-2.123	-1.811	-3.647	-5.654
Magnetic moment		0.972	0.972	1.141	1.416	1.417	1.417	4.871

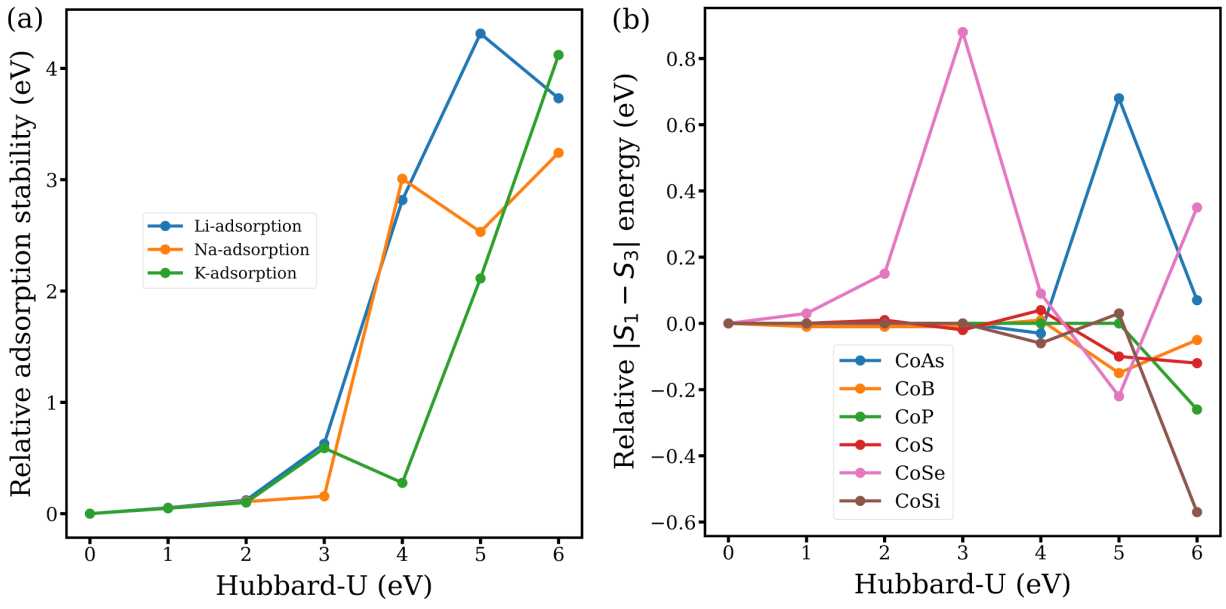

Figure 7. (a) Changes in the adsorption energy of a Li/Na/K-atom on the CoS surface. The energies are reported relative to their corresponding PBE values. (b) Variation in the adsorption energy difference (between the S1 and S3 sites) of a Na atom with 'U'.

Unlike the metallicity and magnetic moment, there is a notable difference in the adsorption energy of a Li/Na/K-atom on the CoS surface with an increase in the U value (see **Table 3**). Although there is an overall increment in the adsorption energy with the U value, the increment is not continuous, i.e., there is an oscillatory behavior. For example, the K-atom adsorption energy value at U = 3 is larger than that at U=4 eV. In **Figure 7a**, we presented the changes in the adsorption energies (relative to the corresponding PBE value) of a Li/Na/K-atom on the CoS surface with an increase in the U value. Clearly, till U=3 eV, the differences are minimal. However, beyond U= 3 eV, the onsite repulsions affect the adsorption energies significantly. As such, these results suggest that if the true U value of the CoS or CoSe anti-MXenes is beyond 3 eV, then the results presented in this report might be affected. Specifically, the SCC and average voltage will be greatly affected. It should be noted that earlier reports on the FeSe anti-MXene also had similar conclusions regarding the adsorption energy variations with the U value.[102] Finally, for NIBs, we repeated these adsorption energy calculations across all systems, and we found similar results. It is interesting to note from these calculations that the adsorption energy differences between the S3 and S1 sites (which dictate the migration energy barriers) did not change considerably with the U value (**Figure 7b)**, with a few exceptions. Thus, we expect that the reported metallicity and MEBs will not be significantly affected by the presence of strong correlations in these materials.

Conclusions

In conclusion, we examined the potential of cobalt anti-MXenes (newly discovered 2D materials) as anode materials for lithium, sodium, and potassium ion batteries by evaluating their structural, electronic, and electrochemical properties. We find that Co-anti-MXenes are electrical conductors and are dynamically stable. The adsorption of alkali metal atoms onto the surface of Co-anti-MXenes is thermodynamically feasible, with calculated adsorption energies that are superior to many other 2D anode materials; in the range of -0.92 to -1.7 eV for Li, -0.79 to -1.7 eV for Na, and -1.26 to -2.22 eV for K. Co-anti-MXenes also have moderate to low migration energy barriers for the alkali metal atoms, indicating the potential for faster charge-discharge kinetics. These barriers, which determine how easily the metal atoms can move within the material, are in the range of 0.4-0.8 eV for LIBs, 0.3-0.6 eV for NIBs, and 0.2-0.4 eV for KIBs. Importantly, contrary to the conventional belief, we found that the strength of adsorption does not necessarily determine the migration energy barrier. Instead, the migration energy is related to the differences in adsorption energies at different sites on the anode material, not their absolute values. Moreover, these differences can be readily used to explain the differences in the MEBs of (i) a metal atom along different paths, (ii) different alkali metal atoms on a specific anode surface, and (iii) the same metal atom across different anode surfaces.

The ability of Co-anti-MXenes to adsorb multiple alkali atoms per formula unit leads to high SCC values and low average anodic voltages. As anode materials for LIBs, CoP and CoSi can provide SCC values of 1075.4 mAh g^{-1} and 934 mAh g^{-1}, and anodic voltages as low as 0.28 V and 0.43 V, respectively. Similarly, for NIBs, Co-anti-MXenes have SCC values in the range of 390-590 mAh g^{-1}, and anodic voltages of around 0.4 V. These SCC values are superior to those of the commercial graphite anode material and many other 2D materials, including MXenes. Moreover, the maximally loaded Co-anti-MXenes are thermally stable and show minimal to moderate volume expansion. However, due to their relatively high average anodic voltages (0.6-1.2 V), and low SCC values ($\leq$ 246 mAh g^{-1}), Co-anti-MXenes may not be suitable as anodes for KIBs. Considering all factors, *we suggest that CoP is*

a promising anode material for all three types of batteries, while CoSi is a promising anode for lithium and sodium-ion batteries. CoB, CoP, and CoS are reasonably good for KIBs, but are promising anode materials for NIBs. Finally, as suggested by our PBE+U calculations, these results could change significantly if these systems are strongly correlated.

Author contributions

Subhadeep Banerjee: Conceptualization, Methodology, Software, Validation, Formal analysis, Investigation, Data curation, Writing – original draft, Writing – review & editing, Visualization; **Ankita Narwal:** Methodology, Software, Validation, Data curation, Investigation; **Sandeep Reddy:** Resources, Validation, Writing – review & editing, Supervision; **Sharma S.R.K.C. Yamijala:** Conceptualization, Methodology, Validation, Formal analysis, Resources, Data curation, Writing – original draft, Writing – review & editing, Visualization, Supervision, Project administration, Funding acquisition.

Conflicts of interest

There are no conflicts to declare.

Acknowledgments

We thank Dr. Jinxing Gu and Prof. Zhongfang Chen for several fruitful discussions. S. B. thanks Vikash Khokhar for his help in preparing the TOC graphic. S.K.R. acknowledges the National Supercomputing Mission (NSM) for providing computing resources of "PARAM Shakti" at IIT Kharagpur, which is implemented by C-DAC and supported by the Ministry of Electronics and Information Technology (MeitY) and Department of Science and Technology (DST), Government of India. S.S.R.K.C.Y. acknowledges the financial support of IIT Madras through the MPHASIS faculty fellowship and through its new faculty support grants NFSG (IP2021/0972CY/NFSC008973), NFIG (RF2021/0577CY/NFIG008973), and DST-SERB (SRG/2021/001455).

References

1 G. L. Soloveichik, Battery technologies for large-scale stationary energy storage, *Annu. Rev. Chem. Biomol. Eng.*, 2011, **2**, 503–527.

2 C. Fu, M. B. Oviedo, Y. Zhu, A. von Wald Cresce, K. Xu, G. Li, M. E. Itkis, R. C. Haddon, M. Chi, Y. Han, B. M. Wong and J. Guo, Confined Lithium-Sulfur Reactions in Narrow-Diameter Carbon Nanotubes Reveal Enhanced Electrochemical Reactivity, *ACS Nano*, 2018, **12**, 9775–9784.

3 C. Fu, B. M. Wong, K. N. Bozhilov and J. Guo, Solid state lithiation-delithiation of sulphur in sub-nano confinement: a new concept for designing lithium-sulphur batteries, *Chem. Sci.*, 2016, **7**, 1224–1232.

4 C. Fu, L. Xu, F. W. Aquino, A. Cresce V., M. Gobet, S. G. Greenbaum, K. Xu, B. M. Wong and J. Guo, Correlating Li-Solvation Structure and its Electrochemical Reaction Kinetics with Sulfur in Subnano Confinement, *J. Phys. Chem. Lett.*, 2018, **9**, 1739–1745.

5 Y. Ding, Z. P. Cano, A. Yu, J. Lu and Z. Chen, Automotive Li-ion batteries: Current status and future perspectives, *Electrochem. energy rev.*, 2019, **2**, 1–28.

6 J. Deng, C. Bae, A. Denlinger and T. Miller, Electric vehicles batteries: Requirements and challenges, *Joule*, 2020, **4**, 511–515.

7 T. Perveen, M. Siddiq, N. Shahzad, R. Ihsan, A. Ahmad and M. I. Shahzad, Prospects in anode materials for sodium ion batteries - A review, *Renewable Sustainable Energy Rev.*, 2020, **119**, 109549.

8 S. S. R. K. C. Yamijala, H. Kwon, J. Guo and B. M. Wong, Stability of Calcium Ion Battery Electrolytes: Predictions from Ab Initio Molecular Dynamics Simulations, *ACS Appl. Mater. Interfaces*, 2021, **13**, 13114–13122.

9 C. Chowdhury, P. Gain and A. Datta, Evolutionary structure prediction-assisted design of anode materials for Ca-ion battery based on phosphorene, *Phys. Chem. Chem. Phys.*, 2021, **23**, 9466–9475.

10 K. Sada, R. Gond, N. Bothra, S. K. Pati and P. Barpanda, Potassium Cobalt Pyrophosphate as a Nonprecious Bifunctional Electrocatalyst for Zinc-Air Batteries, *ACS Appl. Mater. Interfaces*, 2022, **14**, 8992–9001.

11 P. Panigrahi, S. B. Mishra, T. Hussain, B. R. K. Nanda and R. Ahuja, Density functional theory studies of Si_2BN nanosheets as anode materials for magnesium-ion batteries, *ACS Appl. Nano Mater.*, 2020, **3**, 9055–9063.

12 K. Kubota, M. Dahbi, T. Hosaka, S. Kumakura and S. Komaba, Towards K-Ion and Na-Ion Batteries as 'Beyond Li-Ion', *Chem. Rec.*, 2018, **18**, 459–479.

13 W. M. Haynes, *CRC Handbook of Chemistry and Physics*, CRC Press, 2016.

14 E. Wang, Y. Niu, Y.-X. Yin and Y.-G. Guo, Manipulating electrode/electrolyte interphases of sodium-ion batteries: Strategies and perspectives, *ACS Materials Lett.*, 2021, **3**, 18–41.

15 Anoopkumar, B. John and M. Td, Potassium-ion batteries: Key to future large-scale energy storage?, *ACS Appl. Energy Mater.*, 2020, **3**, 9478–9492.

16 H. Wang, D. Yu, C. Kuang, L. Cheng, W. Li, X. Feng, Z. Zhang, X. Zhang and Y. Zhang, Alkali metal anodes for rechargeable batteries, *Chem*, 2019, **5**, 313–338.

17 E. A. Wu, S. Banerjee, H. Tang, P. M. Richardson, J.-M. Doux, J. Qi, Z. Zhu, A. Grenier, Y. Li, E. Zhao, G. Deysher, E. Sebti, H. Nguyen, R. Stephens, G. Verbist, K. W. Chapman, R. J. Clément, A. Banerjee, Y. S. Meng and S. P. Ong, A stable cathode-solid electrolyte composite for high-voltage, long-cycle-life solid-state sodium-ion batteries, *Nat. Commun.*, 2021, **12**, 1256.

18 S. Ghosh, N. Barman, E. Gonzalez-Correa, M. Mazumder, A. Zaveri, R. Giovine, A. Manche, S. K. Pati, R. J. Clément and P. Senguttuvan, Elucidating the Impact of Mg Substitution on the Properties of NASICON‐$Na_{3+y}V_{2-y}Mg_y(PO_4)_3$ Cathodes, *Adv. Funct. Mater.*, 2021, **31**, 2105463.

19 E. Olsson, J. Yu, H. Zhang, H.-M. Cheng and Q. Cai, Atomic‐scale design of anode materials for alkali metal (Li/Na/K)‐ion batteries: Progress and perspectives, *Adv. Energy Mater.*, 2022, **12**, 2200662.

20 S. Banerjee, G. Periyasamy and S. K. Pati, Possible application of 2D-boron sheets as anode material in lithium ion battery: A DFT and AIMD study, *J. Mater. Chem. A*, 2014, **2**, 3856–3864.

21 C. Chowdhury, S. Karmakar and A. Datta, Capping black phosphorene by h-BN enhances performances in anodes for Li and Na ion batteries, *ACS Energy Lett.*, 2016, **1**, 253–259.

22 A. Marzouk, P. B. Balbuena and F. El-Mellouhi, Open framework allotropes of silicon: Potential anode materials for Na and Li-ion batteries, *Electrochim. Acta*, 2016, **207**, 301–307.

23 S. Abdolhosseini, M. Boroun and M. Pourfath, Ab initio analysis of periodic self-assembly phases of borophene as anode material for Na-ion batteries, *J. Phys. Chem. C*, 2021, **125**, 5436–5446.

24 X. Yuan, Z. Chen, B. Huang, Y. He and N. Zhou, Potential applications of MoS_2/M_2CS_2 (M = ti, V) heterostructures as anode materials for metal-ion batteries, *J. Phys. Chem. C*, 2021, **125**, 10226–10234.

25 I. Demiroglu, F. M. Peeters, O. Gülseren, D. Çakır and C. Sevik, Alkali Metal Intercalation in MXene/Graphene Heterostructures: A New Platform for Ion Battery Applications, *J. Phys. Chem. Lett.*, 2019, **10**, 727–734.
26 X. Yuan, Z. Zhang, Y. He, S. Zhao and N. Zhou, Multilayer load and fast diffusion of metal ions on a Ti_2CS_2/blue phosphorene heterostructure anode, *J. Phys. Chem. C*, 2022, **126**, 91–101.
27 J. Gu, Z. Zhao, J. Huang, B. G. Sumpter and Z. Chen, MX Anti-MXenes from Non-van der Waals Bulks for Electrochemical Applications: The Merit of Metallicity and Active Basal Plane, *ACS Nano*, 2021, **15**, 6233–6242.
28 S. Banerjee, K. Ghosh, S. K. Reddy and S. S. R. K. C. Yamijala, Cobalt anti-MXenes as promising anode materials for sodium-ion batteries, *J. Phys. Chem. C*, 2022, **126**, 10298–10308.
29 J. Hao, J. Zheng, F. Ling, Y. Chen, H. Jing, T. Zhou, L. Fang and M. Zhou, Strain-engineered two-dimensional MoS_2 as anode material for performance enhancement of Li/Na-ion batteries, *Sci. Rep.*, 2018, **8**, 2079.
30 Z. Wang, A review on MXene: Synthesis, properties and applications on alkali metal ion batteries, *IOP Conf. Ser. Earth Environ. Sci.*, 2021, **714**, 042030.
31 P. E. Blöchl, Projector augmented-wave method, *Phys. Rev. B Condens. Matter*, 1994, **50**, 17953–17979.
32 G. Kresse and J. Furthmüller, Efficient iterative schemes for ab initio total-energy calculations using a plane-wave basis set, *Phys. Rev. B Condens. Matter*, 1996, **54**, 11169–11186.
33 J. P. Perdew, K. Burke and M. Ernzerhof, Generalized Gradient Approximation Made Simple, *Phys. Rev. Lett.*, 1996, **77**, 3865–3868.
34 M. Ernzerhof and G. E. Scuseria, Assessment of the Perdew–Burke–Ernzerhof exchange-correlation functional, *J. Chem. Phys.*, 1999, **110**, 5029–5036.
35 S. Grimme, S. Ehrlich and L. Goerigk, Effect of the damping function in dispersion corrected density functional theory, *J. Comput. Chem.*, 2011, **32**, 1456–1465.
36 G. Henkelman, B. P. Uberuaga and H. Jónsson, A climbing image nudged elastic band method for finding saddle points and minimum energy paths, *J. Chem. Phys.*, 2000, **113**, 9901–9904.
37 G. Henkelman and H. Jónsson, Improved tangent estimate in the nudged elastic band method for finding minimum energy paths and saddle points, *J. Chem. Phys.*, 2000, **113**, 9978–9985.
38 K. Parlinski, Z. Q. Li and Y. Kawazoe, First-principles determination of the soft mode in Cubic ZrO_2, *Phys. Rev. Lett.*, 1997, **78**, 4063–4066.
39 A. Togo and I. Tanaka, First principles phonon calculations in materials science, *Scr. Mater.*, 2015, **108**, 1–5.
40 D. J. Evans and B. L. Holian, The nose–hoover thermostat, *J. Chem. Phys.*, 1985, **83**, 4069–4074.
41 V. Wang, N. Xu, J.-C. Liu, G. Tang and W.-T. Geng, *Computer Physics Communications*, 2021, 267, 108033.
42 S. P. Ong, W. D. Richards, A. Jain, G. Hautier, M. Kocher, S. Cholia, D. Gunter, V. L. Chevrier, K. A. Persson and G. Ceder, Python Materials Genomics (pymatgen): A robust, open-source python library for materials analysis, *Comput. Mater. Sci.*, 2013, **68**, 314–319.
43 K. Momma and F. Izumi, VESTA: a three-dimensional visualization system for electronic and structural analysis, *J. Appl. Crystallogr.*, 2008, **41**, 653–658.
44 M. Králik, Adsorption, chemisorption, and catalysis, *Chem. Pap.*, 2014, **68**, 1625–1638.
45 Y. Li, N. Li, S. Zhao, J. Fan and J.-J. Kai, Strain-tunable electronic properties and lithium storage of 2D transition metal carbide (MXene) Ti_2CO_2 as a flexible electrode, *J. Mater. Chem. A*, 2020, **8**, 760–769.
46 M. Naguib, J. Come, B. Dyatkin, V. Presser, P.-L. Taberna, P. Simon, M. W. Barsoum and Y. Gogotsi, MXene: a promising transition metal carbide anode for lithium-ion batteries, *Electrochem. commun.*, 2012, **16**, 61–64.
47 Q. Tang, Z. Zhou and P. Shen, Are MXenes promising anode materials for Li ion batteries? Computational studies on electronic properties and Li storage capability of Ti_3C_2 and $Ti_3C_2X_2$ (X = F, OH) monolayer, *J. Am. Chem. Soc.*, 2012, **134**, 16909–16916.

48 D. Sun, M. Wang, Z. Li, G. Fan, L.-Z. Fan and A. Zhou, Two-dimensional Ti 3 C 2 as anode material for Li-ion batteries, *Electrochem. commun.*, 2014, **47**, 80–83.
49 X. Zhou, X. Chen, C. Shu, Y. Huang, B. Xiao, W. Zhang and L. Wang, Two-Dimensional Boron-Rich Monolayer BxN as High Capacity for Lithium-Ion Batteries: A First-Principles Study, *ACS Appl. Mater. Interfaces*, 2021, **13**, 41169–41181.
50 K. Yan, H.-W. Lee, T. Gao, G. Zheng, H. Yao, H. Wang, Z. Lu, Y. Zhou, Z. Liang, Z. Liu, S. Chu and Y. Cui, Ultrathin two-dimensional atomic crystals as stable interfacial layer for improvement of lithium metal anode, *Nano Lett.*, 2014, **14**, 6016–6022.
51 P. Ma, D. Fang, Y. Liu, Y. Shang, Y. Shi and H. Y. Yang, MXene-Based Materials for Electrochemical Sodium-Ion Storage, *Adv. Sci.*, 2021, **8**, e2003185.
52 X. Wang, X. Shen, Y. Gao, Z. Wang, R. Yu and L. Chen, Atomic-scale recognition of surface structure and intercalation mechanism of Ti_3C_2X, *J. Am. Chem. Soc.*, 2015, **137**, 2715–2721.
53 P. Ma, D. Fang, Y. Liu, Y. Shang, Y. Shi and H. Y. Yang, MXene-Based Materials for Electrochemical Sodium-Ion Storage, *Adv. Sci.*, 2021, **8**, e2003185.
54 J. Zhou, X. Zha, X. Zhou, F. Chen, G. Gao, S. Wang, C. Shen, T. Chen, C. Zhi, P. Eklund, S. Du, J. Xue, W. Shi, Z. Chai and Q. Huang, Synthesis and Electrochemical Properties of Two-Dimensional Hafnium Carbide, *ACS Nano*, 2017, **11**, 3841–3850.
55 J. A. Dawson and J. Robertson, *The Journal of Physical Chemistry C*, 2016, 120, 22910–22917.
56 T. Lan, T. Wang, W. Zhang, N.-L. Wu and M. Wei, *Journal of Alloys and Compounds*, 2017, 699, 455–462.
57 D.-X. Song, L. Xie, Y.-F. Zhang, Y. Lu, M. An, W.-G. Ma and X. Zhang, *ACS Applied Energy Materials*, 2020, 3, 7699–7709.
58 M. Acerce, D. Voiry and M. Chhowalla, Metallic 1T phase MoS_2 nanosheets as supercapacitor electrode materials, *Nat. Nanotechnol.*, 2015, **10**, 313–318.
59 X. Tang, D. Zhou, P. Li, X. Guo, B. Sun, H. Liu, K. Yan, Y. Gogotsi and G. Wang, MXene-Based Dendrite-Free Potassium Metal Batteries, *Adv. Mater.*, 2020, **32**, e1906739.
60 M. Naguib, R. A. Adams, Y. Zhao, D. Zemlyanov, A. Varma, J. Nanda and V. G. Pol, Electrochemical performance of MXenes as K-ion battery anodes, *Chem. Commun.* , 2017, **53**, 6883–6886.
61 D. Er, J. Li, M. Naguib, Y. Gogotsi and V. B. Shenoy, Ti_3C_2 MXene as a High Capacity Electrode Material for Metal (Li, Na, K, Ca) Ion Batteries, *ACS Appl. Mater. Interfaces*, 2014, **6**, 11173–11179.
62 P. Lian, Y. Dong, Z.-S. Wu, S. Zheng, X. Wang, S. Wang, C. Sun, J. Qin, X. Shi and X. Bao, Alkalized Ti_3C_2 MXene nanoribbons with expanded interlayer spacing for high-capacity sodium and potassium ion batteries, *Nano Energy*, 2017, **40**, 1–8.
63 X. Ren, Q. Zhao, W. D. McCulloch and Y. Wu, MoS_2 as a long-life host material for potassium ion intercalation, *Nano Res.*, 2017, **10**, 1313–1321.
64 T. Liu, Z. Jin, D.-X. Liu, C. Du, L. Wang, H. Lin and Y. Li, A density functional theory study of high-performance pre-lithiated MS_2 (M = Mo, W, V) Monolayers as the Anode Material of Lithium Ion Batteries, *Sci. Rep.*, 2020, **10**, 6897.
65 J. Jin, G. Deokar, P. M. F. J. Costa and U. Schwingenschlögl, Monolayer C_5N : A promising building block for the anode of K -ion batteries, *Phys. Rev. Appl.*, 2022, **17**, 034055.
66 P. Ganesh, J. Kim, C. Park, M. Yoon, F. A. Reboredo and P. R. C. Kent, *Journal of Chemical Theory and Computation*, 2014, 10, 5318–5323.
67 N. Li, Y. Li, X. Zhu, C. Huang, J.-J. Kai and J. Fan, Theoretical investigation of the structure–property correlation of MXenes as anode materials for alkali metal ion batteries, *J. Phys. Chem. C*, 2020, **124**, 14978–14986.
68 X. Zhang, Z. Yu, S.-S. Wang, S. Guan, H. Y. Yang, Y. Yao and S. A. Yang, Theoretical prediction of MoN_2 monolayer as a high capacity electrode material for metal ion batteries, *J. Mater. Chem. A*, 2016, **4**, 15224–15231.
69 X. Zhang, J. Hu, Y. Cheng, H. Y. Yang, Y. Yao and S. A. Yang, Borophene as an extremely high capacity electrode material for Li-ion and Na-ion batteries, *Nanoscale*, 2016, **8**, 15340–15347.

70 S. Zhao, W. Kang and J. Xue, The potential application of phosphorene as an anode material in Li-ion batteries, *J. Mater. Chem. A*, 2014, **2**, 19046–19052.
71 J. Hu, Y. Liu, N. Liu, J. Li and C. Ouyang, Theoretical prediction of T-graphene as a promising alkali-ion battery anode offering ultrahigh capacity, *Phys. Chem. Chem. Phys.*, 2020, **22**, 3281–3289.
72 Z. Yang, Y. Zheng, W. Li and J. Zhang, Tuning the electrochemical performance of Ti_3C_2 and Hf_3C_2 monolayer by functional groups for metal-ion battery applications, *Nanoscale*, 2021, **13**, 11534–11543.
73 C. Eames and M. S. Islam, Ion Intercalation into Two-Dimensional Transition-Metal Carbides: Global Screening for New High-Capacity Battery Materials, *J. Am. Chem. Soc.*, 2014, **136**, 16270–16276.
74 M. K. Aydinol, A. F. Kohan, G. Ceder, K. Cho and J. Joannopoulos, Ab initiostudy of lithium intercalation in metal oxides and metal dichalcogenides, *Phys. Rev. B Condens. Matter*, 1997, **56**, 1354–1365.
75 Y. Ma, Computer simulation of cathode materials for lithium ion and lithium batteries: A review, *Energy Environ. Mater.*, 2018, **1**, 148–173.
76 A. A. Kuzubov, A. S. Fedorov, N. S. Eliseeva, F. N. Tomilin, P. V. Avramov and D. G. Fedorov, High-capacity electrode material BC3for lithium batteries proposed byab initiosimulations, *Phys. Rev. B*, 2012, **85**, 195415.
77 A. Omidvar, Defective Carbon Nanocone as an Anode Material for Lithium-Ion Batteries, *ACS Appl. Energy Mater.*, 2020, **3**, 11463–11469.
78 J. Song, K. Wang, J. Zheng, M. H. Engelhard, B. Xiao, E. Hu, Z. Zhu, C. Wang, M. Sui, Y. Lin, D. Reed, V. L. Sprenkle, P. Yan and X. Li, Controlling surface phase transition and chemical reactivity of O3-layered metal oxide cathodes for high-performance Na-ion batteries, *ACS Energy Lett.*, 2020, **5**, 1718–1725.
79 T. Broux, F. Fauth, N. Hall, Y. Chatillon, M. Bianchini, T. Bamine, J.-B. Leriche, E. Suard, D. Carlier, Y. Reynier, L. Simonin, C. Masquelier and L. Croguennec, High rate performance for carbon‐coated $Na_3V_2(PO_4)_2F_3$ in Na‐ion batteries, *Small Methods*, 2019, **3**, 1800215.
80 K. M. Abraham, How comparable are sodium-ion batteries to lithium-ion counterparts?, *ACS Energy Lett.*, 2020, **5**, 3544–3547.
81 R. P. Joshi, B. Ozdemir, V. Barone and J. E. Peralta, Hexagonal BC_3: A Robust Electrode Material for Li, Na, and K Ion Batteries, *J. Phys. Chem. Lett.*, 2015, **6**, 2728–2732.
82 B. Ge, B. Chen and L. Li, Ternary transition metal chalcogenides Ti_2PX_2 (X = S, Se, Te) anodes for high performance metal-ion batteries: A DFT study, *Appl. Surf. Sci.*, 2021, **550**, 149177.
83 S.-F. Wang, B.-T. Wang, T. Bo, J.-R. Zhang and F.-W. Wang, Theoretical investigation of Ti2B monolayer as powerful anode material for Li/Na batteries with high storage capacity, *Appl. Surf. Sci.*, 2021, **538**, 148048.
84 H. Yu, W. Lin, Y. Zhang, Y. Li, K. Ding, S. Huang and W. Chen, Exploring the potentials of TiN and TiNX (X = O, F, OH) monolayers as anodes for Li or non-Li ion batteries from first-principles calculations, *RSC Adv.*, 2019, **9**, 40340–40347.
85 N. Khossossi, D. Singh, A. Banerjee, W. Luo, I. Essaoudi, A. Ainane and R. Ahuja, High-Specific-Capacity and High-Performing Post-Lithium-Ion Battery Anode over 2D Black Arsenic Phosphorus, *ACS Appl. Energy Mater.*, 2021, **4**, 7900–7910.
86 S. M. Atashzar, S. Javadian, H. Gharibi and Z. Rezaei, Defective phosphorene as an anode material for high-performance Li-, Na-, and K-ion batteries: a first-principles study, *Nanoscale*, 2020, **12**, 20364–20373.
87 S. Lei, X. Chen, J. Wen, X. Zhou and B. Xiao, Passivated 2D Janus borophene as unique Dirac anodes for Na- and K-ion batteries: A first-principle investigation, *Appl. Surf. Sci.*, 2022, **578**, 151994.
88 Y.-C. Rao, S. Yu, X. Gu and X.-M. Duan, Prediction of MoO2 as high capacity electrode material for (Na, K, Ca)-ion batteries, *Appl. Surf. Sci.*, 2019, **479**, 64–69.
89 D. Linden, of T. N. Linden, T. Reddy, L. David and R. Thomas, *Handbook of Batteries*,

McGraw-Hill Professional, 2002.
90 U. Yorulmaz, İ. Demiroğlu, D. Çakir, O. Gülseren and C. Sevik, A systematical ab-initio review of promising 2D MXene monolayers towards Li-ion battery applications, *J. Phys. Energy*, 2020, **2**, 032006.
91 J. Asenbauer, T. Eisenmann, M. Kuenzel, A. Kazzazi, Z. Chen and D. Bresser, The success story of graphite as a lithium-ion anode material – fundamentals, remaining challenges, and recent developments including silicon (oxide) composites, *Sustainable Energy Fuels*, 2020, **4**, 5387–5416.
92 J. Jia, B. Li, S. Duan, Z. Cui and H. Gao, Monolayer MBenes: prediction of anode materials for high-performance lithium/sodium ion batteries, *Nanoscale*, 2019, **11**, 20307–20314.
93 A. H. Farokh Niaei, T. Hussain, M. Hankel and D. J. Searles, Hydrogenated defective graphene as an anode material for sodium and calcium ion batteries: A density functional theory study, *Carbon N. Y.*, 2018, **136**, 73–84.
94 F. Li, Y. Qu and M. Zhao, Germanium sulfide nanosheet: a universal anode material for alkali metal ion batteries, *J. Mater. Chem. A Mater. Energy Sustain.*, 2016, **4**, 8905–8912.
95 Z. Jian, W. Luo and X. Ji, Carbon Electrodes for K-Ion Batteries, *J. Am. Chem. Soc.*, 2015, **137**, 11566–11569.
96 A. Sibari, Z. Kerrami, A. Kara, M. Hamedoun, A. Benyoussef, O. Mounkachi and M. Benaissa, Adsorption and diffusion on a phosphorene monolayer: a DFT study, *J. Solid State Electrochem.*, 2018, **22**, 11–16.
97 K. Fan, Y. Ying, X. Li, X. Luo and H. Huang, Theoretical investigation of V_3C_2 MXene as prospective high-capacity anode material for metal-ion (Li, Na, K, and ca) batteries, *J. Phys. Chem. C*, 2019, **123**, 18207–18214.
98 Y. Xie, Y. Dall'Agnese, M. Naguib, Y. Gogotsi, M. W. Barsoum, H. L. Zhuang and P. R. C. Kent, Prediction and Characterization of MXene Nanosheet Anodes for Non-Lithium-Ion Batteries, *ACS Nano*, 2014, **8**, 9606–9615.
99 Y. Shen, J. Liu, X. Li and Q. Wang, Two-Dimensional T-NiSe as a Promising Anode Material for Potassium-Ion Batteries with Low Average Voltage, High Ionic Conductivity, and Superior Carrier Mobility, *ACS Appl. Mater. Interfaces*, 2019, **11**, 35661–35666.
100 O. Lenchuk, P. Adelhelm and D. Mollenhauer, New insights into the origin of unstable sodium graphite intercalation compounds, *Phys. Chem. Chem. Phys.*, 2019, **21**, 19378–19390.
101 W. Zhang, S. Liu, J. Chen, F. Hu, X. Wang, H. Huang and M. Yao, Exploring the Potentials of TiCNT (= 0, 1, 2)-MXene for Anode Materials of High-Performance Sodium-Ion Batteries, *ACS Appl. Mater. Interfaces*, 2021, **13**, 22341–22350.
102 X. Lv, F. Li, J. Gong, J. Gu, S. Lin and Z. Chen, Metallic FeSe monolayer as an anode material for Li and non-Li ion batteries: a DFT study, *Phys. Chem. Chem. Phys.*, 2020, **22**, 8902–8912.

Table of Contents Graphic

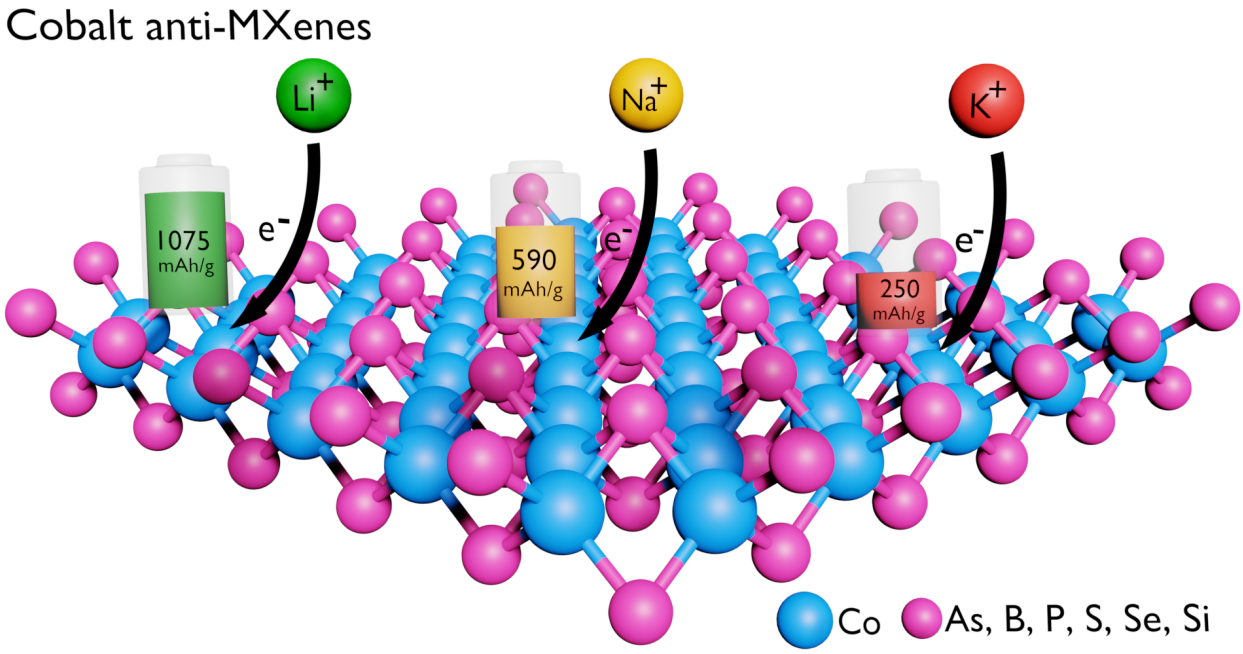

TOC Text: Cobalt anti-MXenes are a new class of 2D materials that can act as promising anode materials for alkali metal ion batteries. They exhibit high specific charge capacities and low migration energy barriers for alkali metal ions.